BULLETIN OF THE POLISH ACADEMY OF SCIENCES
TECHNICAL SCIENCES, Vol. 73(6), 2025, Article number: e154288
DOI: 10.24425/bpasts.2025.154288

Funicular shaping method in the iterative design of reinforced concrete arches with variable cross-sections in urban areas

Tomasz STĘPLOWSKI*

Wrocław University of Science and Technology, Faculty of Civil Engineering, Wybrzeże Stanisława Wyspiańskiego 27, 50-370 Wrocław, Poland

Abstract. This article presents the application of the funicular design method in an iterative process for reinforced concrete arches with variable cross-sections in urban environments. The study aimed to develop an optimal arch shape through multi-criteria optimization that minimizes tensile stresses, structural deflections and material volume. The geometry adapts to the internal force flow by aligning the spatial configuration and ensuring structural efficiency. The method builds on Hooke's observation: "As hangs the flexible line, so, but inverted, will stand the rigid arch". It is further supported by nonlinear numerical analysis conducted using the finite element method that considers second-order effects, creep, concrete shrinkage and geometric imperfections. The results show that the designed arch requires only structural reinforcement, confirming the method's effectiveness. Various modes of arch stability loss were also evaluated. Such structures are commonly used in urban environments, serving both functional and aesthetic purposes. In the context of rapidly developing cities, this article emphasizes the role of digital transformation in structural design. It presents how graphic statics can be integrated with advanced computational tools to streamline workflows and enhance the design process.

Keywords: funicular polygon; force polygon; general method; nonlinear analysis; urban areas.

1. INTRODUCTION

The arch, a fundamental architectural and structural element, has played a pivotal role in shaping buildings across various epochs. Its use in Roman aqueducts and contemporary structures such as bridges, stadiums and halls stands as testament to its enduring engineering solutions. The arch's high efficiency, derived from its favorable static properties, reduces internal forces to a compressive force under eccentric loading, ensuring stresses of the same sign in each cross-section of the structure. Historically, structural arches were primarily constructed from stone or brick, whereas modern designs increasingly utilize steel and reinforced concrete. In dense urban environments, rational structural design supports sustainable development by reducing energy consumption, material use and construction costs [1]. Contemporary structural design trends focus on achieving lightweight solutions that use minimal materials to obtain large spans [2]. As noted by A.R. Kulkarni and V. Bhusare [3], conventional design approaches often rely on excessive material usage. Funicular shaping improves structural efficiency and enables material savings, which is especially beneficial in contexts with strict economic limitations.

Static analyses can be carried out using both analytical and graphical methods. The foundations of graphic statics date back to early studies on the free fall of bodies under the influence of gravity forces conducted by Leonardo da Vinci and Galileo [4]. Simon Stevin (1548–1620) was the first to represent a force as a vector. He was the author of the parallelogram principle, in which he proved that the equilibrium of a system could be presented graphically utilizing a closed polygon of forces [5]. This trend initiated the development of graphical methods for analyzing the equilibrium of structural systems. The French scientist Pierre Varignon (1654–1722), in a publication released posthumously in 1725 titled *Nouvelle mécanique ou Statique* (translated as "New Mechanics or Statics"), presented concepts that significantly contributed to the development of structures created in a funicular manner. The essence of this approach lies in the relationship between its two main pillars: force polygon and funicular polygon [6].

In 1675, English scientist Robert Hooke introduced a completely different perspective on the use of the arch in building structures, which he summarized in a single statement: "As hangs the flexible line, so, but inverted, will stand the rigid arch". Research inspired by Robert Hooke's observations provided a foundation for the development of graphic statics, which enhanced the understanding of the static behavior of arches and their deliberate use in historical and modern buildings [7].

R. Rozendaal and A. Borgart, in [8], described a new method for calculating arches using graphic statics, which is based on minimizing the complementary energy resulting from bending moments. It was assumed that the complementary energy resulting from the normal force is negligible and the thickness of the arch remains constant along its entire length. However, for complex, non-prismatic arches, the proposed equation turns out to be difficult to apply.

*e-mail: tomasz.steplowski@pwr.edu.pl

Manuscript submitted 2025-02-12, revised 2025-05-02, initially accepted for publication 2025-05-03, published in November 2025.

The work by G. Tempesta and S. Galassi [9], along with the developed MATLAB code [10], serves as an essential reference, as it introduces a numerical approach to evaluating the safety of masonry arches by computing the thrust line closest to the geometrical axis. This study translates the graphical thrust line method into a numerical procedure, allowing for an analytical interpretation. Although focused on masonry structures, it underscores the importance of graphical and numerical techniques in assessing the internal force flow within arch systems. Similarly, in the design of reinforced concrete arches, the funicular shaping method can be employed to achieve an optimized geometry that aligns with internal force trajectories.

This paper presents an approach that combines graphic statics with a modern design procedure utilizing the finite element method (FEM). The proposed integration establishes a clear relationship between the initial input data and the calculation results, offering an intuitive workflow for shaping reinforced concrete arches. The innovative aspect of this study lies in merging the funicular shaping method with nonlinear structural analysis, enabling the design of geometrically optimized and materially efficient arch forms tailored to complex loading conditions. In this context, sustainability refers to reducing the volume of concrete used, lowering energy consumption during construction, and minimizing the environmental impact while ensuring long-term durability. The concept of optimality adopted in this study is formalized as a multi-objective optimization task that aims to minimize structural deflections, tensile stresses, and material volume, all while satisfying strength and stability constraints.

The numerical analysis of the arch was carried out in software [11], using the general method described in [12], which consisted of performing a complete nonlinear analysis of the structure considering geometric and material nonlinearity. Eurocode 2 requires that in addition to initial imperfections, the influence of creep and cracking should also be taken into account. The impact of long-term effects was considered utilizing the σ-ε diagram, following the guidelines for nonlinear analysis of structures, multiplying the deformations by the effective creep coefficient. Due to the absence of specific guidelines in [12] for determining the initial deformation of the arch, standards for timber structures [13] and steel bridges [14] were applied, along with the newly introduced second-generation Eurocode 2 [15], which was utilized in the final stage of the work. Subsequently, linear bifurcation analysis (LBA) was performed, followed by rescaling the first and third modes of stability loss, according to the guidelines from the specified standards. In this manner, the initial imperfection was taken into account. A high convergence of the modes of arch stability loss from two independent software tools SOFiSTiK and Dlubal RFEM [11, 16] was also found. Moreover, the calculations were designed to achieve a result where the stresses in each cross-section had the same sign, enabling the effects of cracking and stress redistribution to be disregarded. Based on the funicular approach, the method applied resulted in a shape that optimally aligned with the flow of internal forces.

The application of the hanging chain principle has had a profound impact on historical engineering and architectural works, offering a foundational approach to form optimization. One of the earliest and most remarkable applications of this method was by Antoni Gaudí. In the crypt of the Colònia Güell church, Gaudí developed two- and three-dimensional physical models to define the geometry of arches and vaults through the natural catenary shapes formed by suspended chains [17, 18]. His pursuit of structural efficiency through form continued in the Sagrada Familia (shown in Fig. 1), where the design reflects an understanding of force flow and the optimization of structural elements [19].

Fig. 1. Exterior view of the Sagrada Familia in Barcelona. Photo by the author

Similarly, an early application of reinforced concrete in urban public architecture in Wrocław can be observed in the Wrocław Market Hall (shown in Fig. 2), constructed between 1907 and 1908, based on a design by Richard Plüddemann and Heinrich Küster. This structure was among the first in Europe to utilize parabolic reinforced concrete arches with a significant span of approximately 19 meters [20]. The parabolic arches of the Market Hall represent a pioneering step towards structural forms shaped by the natural flow of internal forces, anticipating the monumental reinforced concrete achievements later realized in Max Berg's Centennial Hall. Furthermore, studies on early twentieth-century concrete structures in Wrocław confirm that despite limited initial knowledge about reinforced concrete behavior under various environmental influences, many such elements, including those in the historic Market Hall, continue to demonstrate remarkable durability after more than a century of service [21].

The progression toward a fully optimized architectural form culminated in the Centennial Hall in Wrocław, completed in 1913 and inscribed onto the UNESCO World Heritage List in 2006. This iconic structure stands as a landmark of 20th-century architecture. Max Berg led the architectural vision,

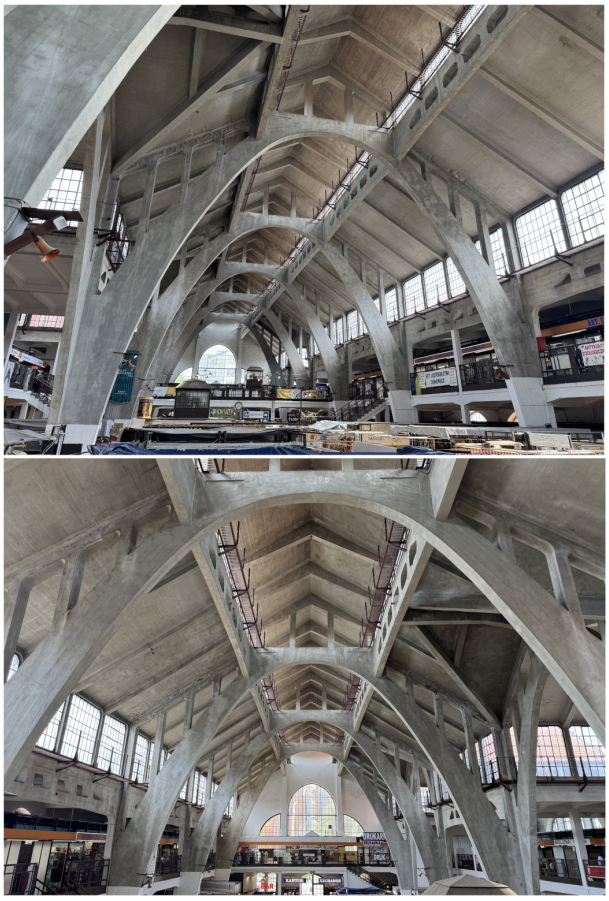

Fig. 2. Interior views of the Wrocław Market Hall. Photos by the author

with structural expertise provided by Günther Trauer and Willy Gehler [22]. The structural system of the Centennial Hall reflects a deliberate attempt to achieve an optimized form that efficiently distributes internal forces within the concrete structure.

2. RESEARCH SIGNIFICANCE

The objective of this study is to explore how integrating traditional graphic statics with advanced nonlinear numerical techniques can enhance the design and analysis of reinforced concrete arches. Rather than replacing classical tools, this approach extends their applicability to modern engineering practice by embedding them into a computational optimization framework. The significance of this research lies in its potential to bridge the gap between intuitive form-finding and rigorous numerical validation.

This integration addresses the growing need for design methodologies that combine transparency with analytical robustness. Such methodological synergy is increasingly emphasized in contemporary approaches to sustainable urban development [23]. Furthermore, the study responds to the increasing demand for tools that support multi-criteria assessment of complex geometries. Such tools allow engineers to evaluate structural performance, resource efficiency and long-term durability within a unified framework. While the funicular method itself is well-established, its focused application to constrained urban contexts, combined with iterative refinement through nonlinear analysis, represents a novel and practically relevant design strategy. The motivation for this research stems from contemporary challenges related to reducing material consumption, minimizing environmental impact, and lowering construction costs, while simultaneously improving structural longevity and reliability.

Such an approach reflects the ongoing digital transformation of structural design processes, wherein traditional methods are enhanced by computational tools to achieve optimized structural forms [17]. In parallel, the funicular approach contributes to sustainable construction by minimizing material use. This aligns with broader low-carbon design strategies that also address embodied carbon [24, 25].

3. METHODOLOGY

3.1. Graphical shaping method

The funicular method in graphic statics employs two interrelated diagrams. The first is the funicular polygon, which represents the geometry of the structure. The second is the force polygon, which reflects the state of force equilibrium. Loads are first defined and applied in order to construct the force polygon, from which the funicular polygon is derived. The precision of this method depends on the discretization of the arch, since smaller segments yield more accurate results. Each segment of the structure corresponds to a vector in the force polygon, whose direction and magnitude reflect internal forces. Radial lines from the pole "O" to the load points define the force flow, and their lengths represent the axial forces in the structure. When the resulting polygon closes, the structure is in equilibrium [4, 26], as shown in Fig. 3.

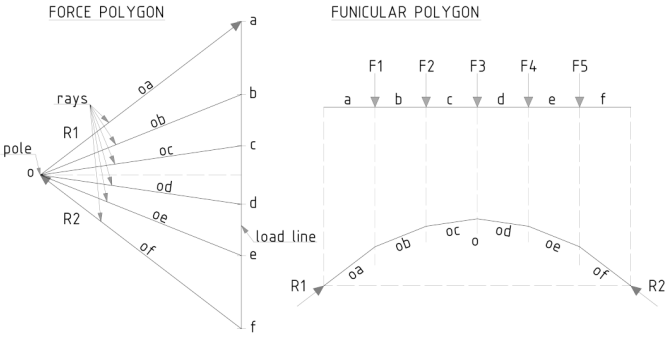

Fig. 3. Graphical construction of a funicular polygon derived from a force polygon

This method simulates how a structure adapts to gravitational or lateral loading. The location of the pole relative to the load line determines the resulting shape. Moving the pole closer to the load line increases the rise of the arch and simultaneously reduces internal force magnitudes. The method accommodates both symmetric and asymmetric loading conditions, with force magnitude visually represented by the spacing between load

points. Gravitational loads appear as vertical lines, whereas wind or lateral loads form inclined segments in the force polygon [4, 26], as depicted in Fig. 4.

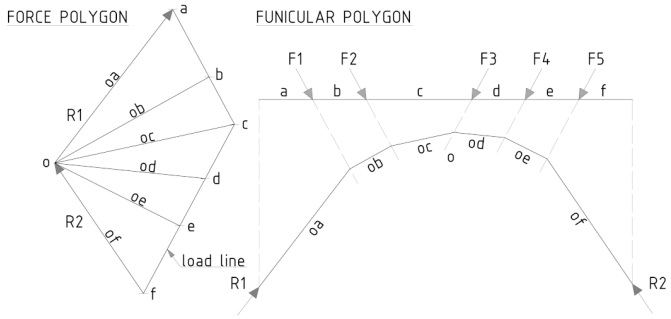

Fig. 4. Influence of inclined forces on the shape of funicular polygons

According to Stevin's principle, a convergent force system reaches static equilibrium when the polygon of forces is closed. Each node satisfies equilibrium when the vector sum of forces in both axes equals zero, forming triangular force chains [4,26], as shown in Fig. 5.

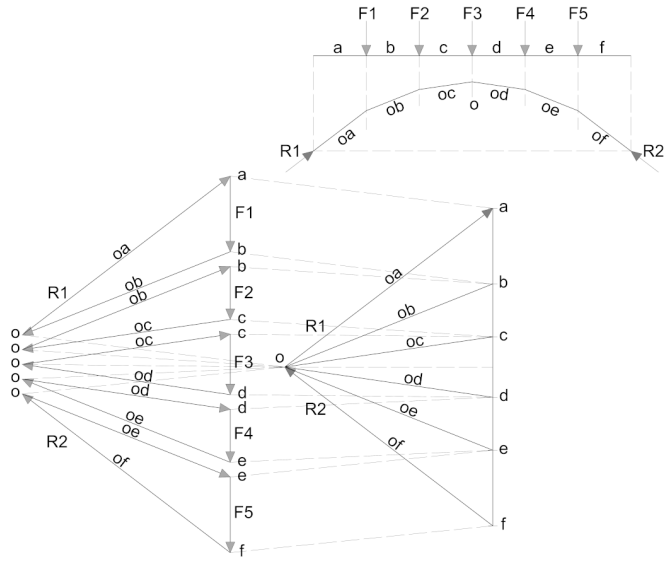

Fig. 5. Each node of a funicular structure forms a closed triangle on the force polygon

This graphical approach forms the basis for further numerical refinement, integrating traditional methods into a modern optimization workflow.

3.2. Nonlinear structural analysis

Building upon the results of the graphical method, the analysis is further extended using a nonlinear computational approach. In accordance with [12], which permits nonlinear methods of analysis for both the ultimate limit state (ULS) and the serviceability limit state (SLS), provided that equilibrium, compatibility and realistic material behavior are ensured, this stage aims to refine and verify the structural response of the arch. This approach involves nonlinear physical laws, which exhibit particular complexity in the case of reinforced concrete. The primary source of this nonlinearity lies in the nonlinear relationships between stress and strain. Additionally, structural analysis may involve nonlinear geometric relationships, referred to as second-order analysis, which accounts for the influence of displacements on the distribution of internal forces and stresses, and consequently, on the final deformations and displacements [12,27]. Considering second-order effects is crucial due to the slenderness of the structure being designed, which is primarily subjected to compressive forces. In the context of the main objective of this study, which is the design of a structure with optimized geometry, the application of nonlinear analysis is fully justified. Its fundamental advantage is the ability to obtain more realistic distributions of internal forces and displacements, leading to a more accurate assessment of the structure's safety level.

3.3. Mathematical background formulation of the optimization problem

The optimization problem is formulated as a multi-objective task involving the selection of design variables that define the geometry of the structure – both the shape of the arch axis and the variation of its cross-section – with the goal of minimizing the objective function $f(x)$, subject to constraints that define the set of admissible solutions.

The decision variable $x \in \mathbb{R}^n$ represents a vector in the n-dimensional space of real-valued geometric parameters that describe the structure, and is defined as:

$$x = \left[x_1,\ x_2,\ \ldots,\ x_n\right]^{\mathrm{T}}. \tag{1}$$

Each component x_i of the vector x represents a coefficient in the functions that describe the geometry of the arch axis (e.g. in polynomial form), and the variable height of the cross-section along the arch length. The optimization task consists in minimizing the objective function over the admissible set $D \subset \mathbb{R}^n$, and is expressed as:

$$\min f(x) = \left[f_1(x),\ f_2(x),\ f_3(x)\right]^{\mathrm{T}}, \quad \text{for } x \in D, \tag{2}$$

subject to the following constraints:

$$g_i(x) \le 0, \quad \text{for} \quad i = 1,2,\ldots,m, \tag{3}$$

where the functions $g_i(x)$ represent structural constraints, including strength, geometric and stability requirements. The set D denotes the design space, i.e. the domain of admissible design solutions satisfying all imposed constraints.

The objective criteria considered are as follows:

- Minimization of the maximum deflection of the structure:

$$f_1(x) = \max\left\{|u(s,x)| : s \in (0, L),\ x \in D\right\}. \tag{4}$$

- Minimization of maximum tensile stress:

$$f_2(x) = \max\left\{\sigma_t(s,x) : s \in (0, L),\ x \in D\right\}. \tag{5}$$

- Minimization of the structure's total volume (with variable height and constant width b):

$$f_3(x) = V(x) = \int_0^L A(s,x)\,\mathrm{d}s, \quad \text{for } x \in D, \tag{6}$$

$$\text{where: } A(s,x) = b \cdot h(s,x). \tag{7}$$

Assumed notations:

- $s \in (0, L)$ – arc-length coordinate (length measured along the axis of the arch),
- $u(s,x)$ – deflection of the structure at point s,
- $\sigma_t(s,x)$ – tensile stress in the cross-section,
- $h(s,x)$ – variable height of the cross-section,
- $A(s,x)$ – cross-sectional area,
- b – constant width of the cross-section.

The optimization problem described is solved using a funicular-based design approach, in which the geometry of the structure is generated through graphic statics.

4. GRAPHICAL DETERMINATION OF THE OPTIMAL SHAPE BASED ON FORCE FLOW ANALYSIS

All loads used in the analysis are summarized in Table 1. The assumptions are based on relevant building standards, the specific characteristics of local climatic conditions, and current engineering practice. The design loads were established to determine the optimal shape of the arch. After defining the geometry, a spatial model will be developed to calculate the actual load distribution.

Permanent actions, including the self-weight of structural elements and material layers, were determined using standard volumetric densities and representative layer thicknesses. Reinforced concrete was assumed with a density of 25.0 kN/m^3, cement screed with 24.0 kN/m^3, and mineral wool with 1.6 kN/m^3. The roof covering consists of a PVC membrane, mineral wool insulation, polyethylene foil and trapezoidal sheet metal. The floor build-up includes laminated panels, cement screed, separation and insulation layers, a reinforced concrete slab, plaster and suspended ceiling. Technological loads related to installations (pipes, cables, ducts) were estimated at 0.25 kN/m^2 based on catalog data. The load from movable partition walls ($\leq$ 3.0 kN/m of wall length) was included according to [28] and incorporated as uniformly distributed permanent load of 1.20 kN/m^2. Roof live load and floor operational loads were taken from EN 1991-1-1, corresponding to load categories H and C3, respectively. Snow and wind actions were adopted according to [29] and [30], with the building located in Wrocław (Poland), in snow zone 1 and wind zone 1. The characteristic ground snow load was assumed as 0.70 kN/m^2 and basic wind velocity was 22.0 m/s. The inclination angle of the roof was taken as 30°, with exposure and shape coefficients applied as per Eurocode provisions. The initial cross-sections of the roof structure in the central bay were determined based on the condition of limiting compressive stress in concrete, assuming class C30/37, in order to control cracking and creep under long-term loading.

4.1. Funicularly shaped form of a reinforced concrete hall

Two structural variants of the reinforced concrete hall are analyzed in this study. Variant I features a single-nave layout with a central funicular arch serving as the main load-bearing element. Variant II introduces a three-nave configuration with three parallel arches supporting the roof structure. Figures 6 and 7 illustrate the loads assumed, internal force diagrams, and resulting arch geometries for both structural variants.

Table 1
Design assumptions adopted

Type of load	Description	Load value	Unit	Notes
Structure dead loads	Self-weight of the roof support structure	–	–	Reinforced concrete purlins, posts and joists
	Self-weight of the arch girder	–	–	The first iteration assumed a prismatic arch cross-section of 100 × 100 cm
	Flat roof layers	0.371	kN/m^2	PVC roof membrane, welded, mineral wool, PE polyethylene foil, trapezoidal sheet metal
	Floor layers	8.338	kN/m^2	Laminated panels, cement screed reinforced with mesh, separation layer – PE foil, sound-absorbing polystyrene, reinforced concrete slab, cement-lime plaster, suspended ceiling
Technological constants	Installations	0.250	kN/m^2	Pipes, cables, ducts
Operational constants	Roof live load	0.400	kN/m^2	According to the standard [28]: Category H
	Maintenance live load	4.000	kN/m^2	According to the standard [28]: Category C3
	Self-weight of movable partition walls	1.200	kN/m^2	According to the standard [28]: movable partition walls with self-weight $\leq$ 3.0 kN/m wall length
Climatic constants	Snow	0.560	kN/m^2	Snow zone I, characteristic value [29]
	Wind	0.553	kN/m^2	Wind zone 1, characteristic value [30]

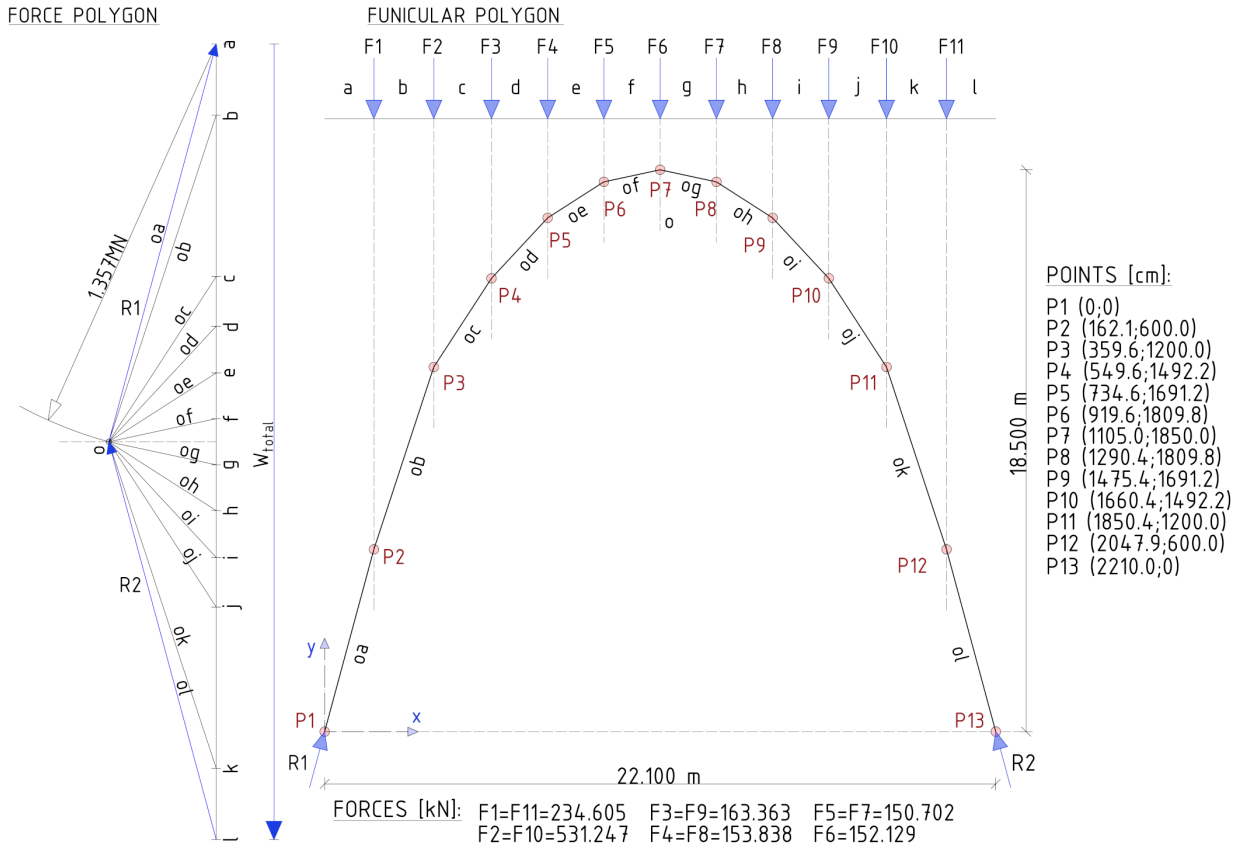

Fig. 6. Funicular model of the main load-bearing structure – variant I

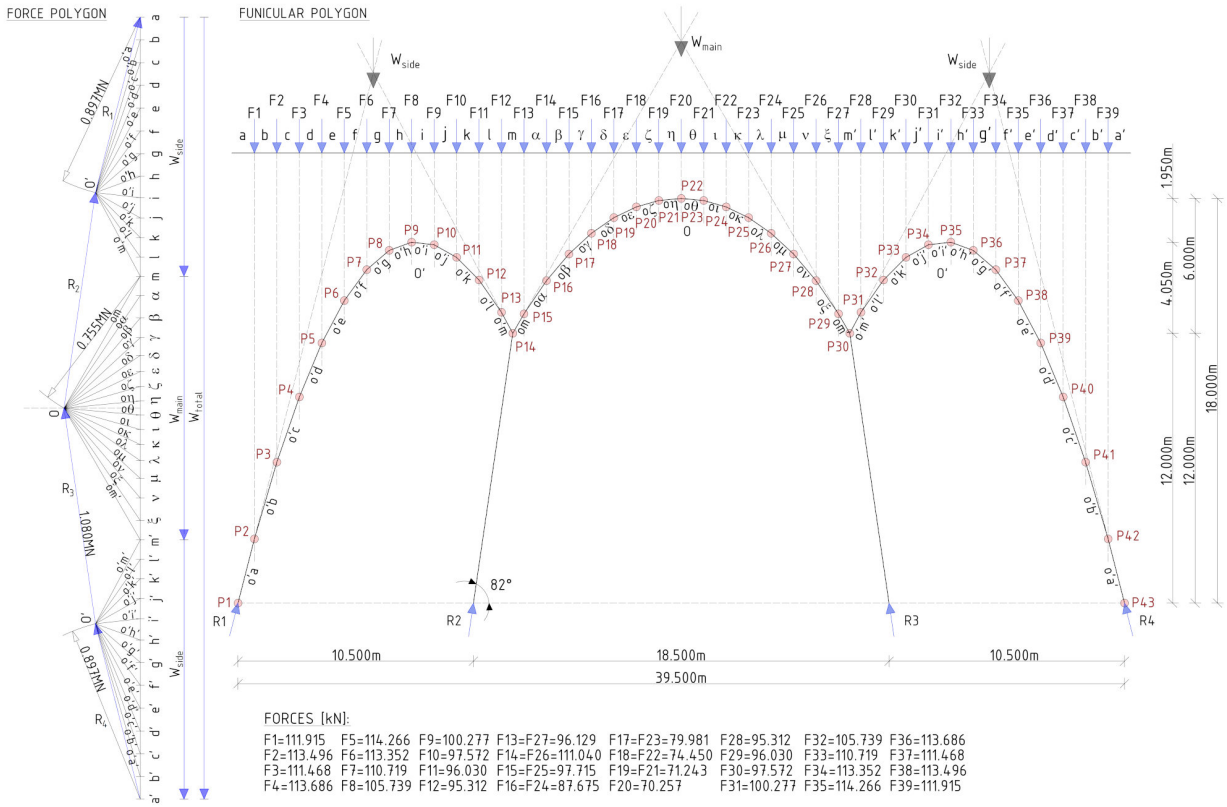

Fig. 7. Funicular model of the main load-bearing structure – variant II

Variant I was selected for further analysis due to its benefits in constructability, cost efficiency, and avoidance of additional measures, such as snow and rain load protection in the side bays.

Graphically estimating the coordinates that characterize the arch shape made it possible to identify the function that best fits the corresponding points, as illustrated in Fig. 8. Wolfram Mathematica [31] was used for this purpose. The results obtained are presented below. Function approximating the final arch shape:

$$f(x) = 4.52722x - 0.420464x^2 + 0.0195632x^3 - 0.000443753x^4. \quad (8)$$

The error resulting from the approximation, which describes the deviation of the approximation function from the coordinates defined graphically, is: $\Delta = -1.42109 \cdot 10^{-14}$.

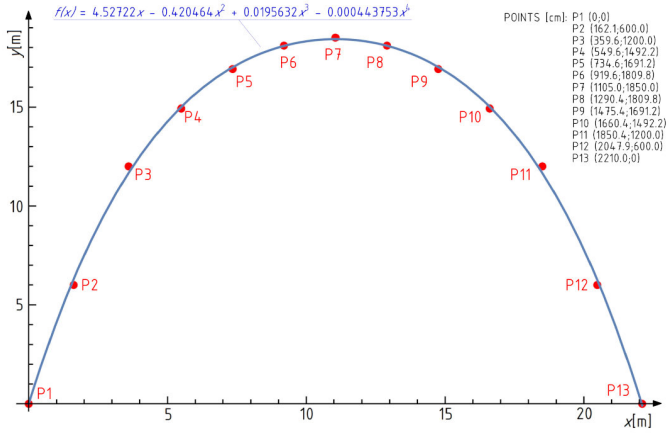

Fig. 8. Graph of the arch geometry defined by function $f(x)$, based on selected geometric coordinates [m]

This error was considered acceptable, therefore, the indicated mathematical function accurately reproduces the shape obtained using a funicular polygon, suggesting that it will faithfully correspond to the design assumptions.

4.2. Arch girder model. Comparison of results using the finite element method

The static diagram of the arch in program [11] is shown in Fig. 9a, and the results of FEM calculations are shown in Fig. 9b.

The values of forces in individual girder segments obtained from two independent methods are similar. The difference of approximately 0.2 kN results from error $\Delta = -1.42109 \cdot 10^{-14}$ of the function, which approximates points obtained through the funicular method by iterating the optimal shape of the girder. The relative error of the two methods is: $\delta = \pm 0.01$.

Finally, the cross-section of the arch was designed as non-prismatic:

– cross-section height:

$$h(x) = 1.0 - 0.0904977x + 0.00409492x^2, \quad (9)$$

– cross-section width: b = constant = 0.50 m.

The final shape of the reinforced concrete arch is shown in Fig. 10.

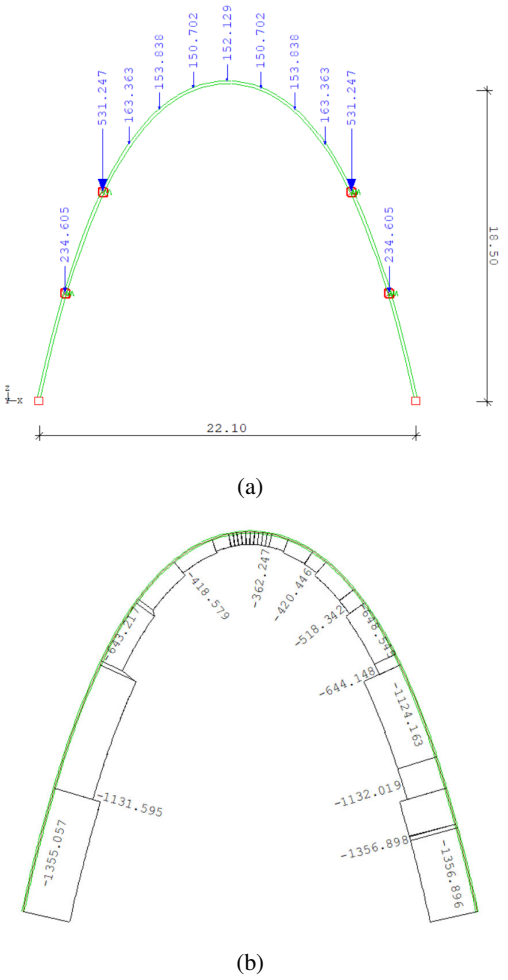

Fig. 9. Static diagram of the arch structure and distribution of axial forces: (a) load diagram and geometric dimensions, (b) axial force diagram N_x [kN]

Fig. 10. Final design of the reinforced concrete arch

4.3. Nonlinear analysis as the general calculation method

The general method is based on second-order nonlinear analysis. Stress-strain relationship for concrete given in Fig. 11 was used. The general principles of nonlinear analysis of structures are given in [12]:

- stress-strain diagrams are based on the calculated values,
- mean value of concrete cylinder compressive strength f_{cm} = 38 MPa, replaced by the value of the design compressive strength:

$$f_{cd} = \frac{30\ \text{MPa}}{1.40}, \tag{10}$$

- modulus of concrete elasticity E_{cm} = 33 GPa was replaced by the value:

$$E_{cd} = \frac{E_{cm}}{\gamma_{CE}} = \frac{32837\ \text{MPa}}{1.20}, \tag{11}$$

- the effect of creep is accounted for by multiplying all strain values in the stress-strain diagram by the appropriate factor $(1+\varphi_{ef})$, as illustrated in Fig. 11.

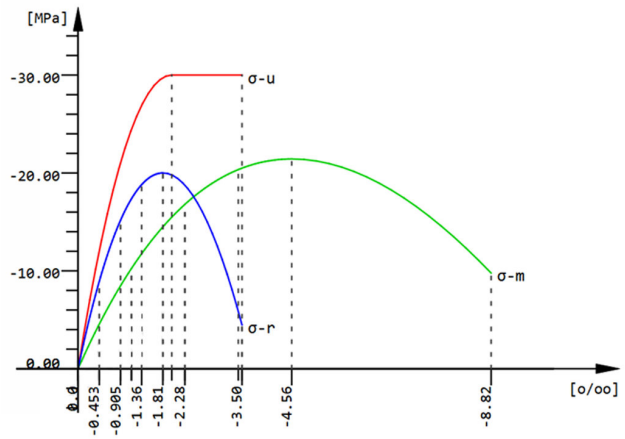

Fig. 11. Stress-strain curve (green color) in the ultimate limit state for C30/37 concrete, scaled by the requirements of the general method for nonlinear structural analysis. The axes represent stress [MPa] and strain [‰]

At the time of the initial loading, corresponding to the concrete age t_0, the compressive stress in the concrete does not exceed $0.45 f_{ck}(t_0)$. Therefore, the final value of the creep coefficient was taken from Fig. 3.1 of standard [12] as $\phi(\infty, t_0) = 2.400$. According to [12], the effective creep ratio is calculated as:

$$\varphi_{ef} = \phi(\infty, t_0)\frac{M_{0Eqp}}{M_{0Ed}} = 1.520, \tag{12}$$

where:
- M_{0Eqp} is the first-order bending moment in quasi-permanent load combination (SLS),
- M_{0Ed} is the first-order bending moment in design load combination (ULS).

This leads to the final form of the coefficient:

$$(1+\varphi_{ef}) = (1+1.52) = 2.520, \tag{13}$$

The total shrinkage strain was calculated according to [12]:

$$\begin{aligned}\varepsilon_{cs} &= \varepsilon_{ca}(t) + \varepsilon_{cd}(t) = 4.715 \cdot 10^{-5} + 1.052 \cdot 10^{-4} \\ &= 1.524 \cdot 10^{-4} = 0.152‰,\end{aligned} \tag{14}$$

where:
- $\varepsilon_{ca}(t)$ is the autogenous shrinkage strain,
- $\varepsilon_{cd}(t)$ is the drying shrinkage strain.

Due to the lack of guidelines in standard [12] regarding the determination of the initial deformation of a reinforced concrete arch, standards [13] and [14], as well as the newly introduced standard [15], were used for this purpose, as summarized in Table 2.

Table 2
Determination of the initial imperfection value of the reinforced concrete arch

Buckling type	Source	Shape of imperfection	Amplitude e_0
Out-of-the plane of the arch	[14]	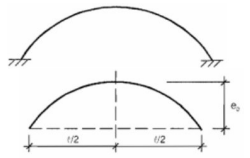	e_0 = 59.60 mm
	[15]	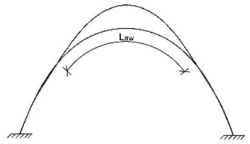	e_0 = 19.48 mm
In the plane of the arch	[14]	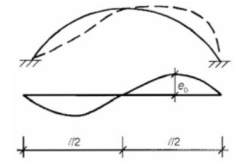	e_0 = 44.20 mm
	[13]	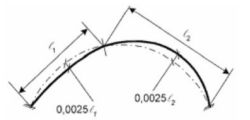	e_0 = 52.50 mm
	[15]	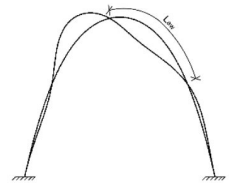	e_0 = 16.07 mm

In the end, out-of-plane imperfections with an amplitude of e_0 = 59.60 mm and in-plane imperfections with an amplitude of e_0 = 52.50 mm were adopted. The implementation of the general method conditions for nonlinear analysis was performed in SOFiSTiK [11]. Below is an excerpt from the script that defines the key parameters and relationships necessary for the design and analysis of the reinforced concrete arch, as shown in Fig. 12a. It also includes the scaling of the appropriate buckling mode so that initial imperfections are taken into account, as illustrated in Fig. 12b.

Figures 12a and 12b present selected excerpts from the computational script, illustrating the definition of geometry, material parameters and analysis settings. For improved clarity, the

```
+prog aqua urs:1
head Material and cross sections
norm en 199X-200X unit 0
echo full full
$ Material
conc 1 type C 30 fcr 30/1.4 ecr 32837/1.2
ssla eps serv epss 2.520
mext 1 exp 1 type eigs val1 -1
$stee 2 type B clas '500B'
$ Sections
#define n=51   //number of elements
#define div=0.221  // division length
let#no=1    //section number
let#x=0     //x coordinate
loop $(n)
    srec #no h 1-0.0904977*#x+0.00409492*#x^2 b 0.5 mno 1
    let#no=#no+1
    let#x=#x+$(div)
endloop
end
```

(a)

```
+prog ase urs:4
head Linear analysis
syst prob line
lc 1
end
+prog ase urs:5
head LBA
syst prob line plc 1
eige 10 etyp buck lc 101
end
+prog ase urs:6
head Imperfection out of plane
syst prob line
obli lc 101 vmax 59.6[mm]
lc 201 dlz 1e-4
end
+prog ase urs:7
head Analysis with both imperfections
syst prob th3 plc 201 iter 200
nstr kmod k1 ksv sl
obli lc 103 vmax 52.5[mm]
lc 202
lcc 1
end
```

(b)

Fig. 12. Implementation of nonlinear analysis in arch design: (a) definition of general method conditions, (b) execution of complete nonlinear structural analysis with scaling of the appropriate buckling mode

corresponding algorithmic logic is also presented in the form of textual pseudocode listings, which provide a simplified and structured representation of the procedures implemented.

Algorithm 1. Definition of the general method conditions for nonlinear arch analysis (based on Fig. 12a)

1. Start the SOFiSTiK module for material and section definition,
2. Set the design code: Eurocode 2 (EN 1992),
3. Define the unit system: system 0,
4. Enable full output display,
5. Define concrete class C30:
   - compressive strength for nonlinear analysis: $f_{cr} = 30.0/1.4$ MPa,
   - elastic modulus for serviceability: $E_{cr} = 32837/1.2$ MPa,
   - scaling factor for σ-ε diagram: 2.520,
6. Do not define an explicit time-shrinkage curve. Shrinkage is modeled analytically as a predefined axial strain: $\varepsilon_{cs} = 0.152‰$(sum of autogenous and drying shrinkage),
7. Define reinforcement: steel class B500B,
8. Set discretization parameters:
   - number of elements: $n = 51$,
   - element length: $div = 0.221$ m,
9. Initialize counters:
   - section number: $no = 1$ and arch position: $x = 0.0$,
10. Loop over all elements:
    - calculate cross-section height: $h(x) = 1 - 0.0904977x + 0.00409492x^2$,
    - assign constant section width: $b = 0.5$ m,
    - increment section number and advance to the next point along the arch,
11. End loop and finalize definition.

Algorithm 2. Definition of complete nonlinear structural analysis with scaling of the appropriate buckling mode (based on Fig. 12b)

1. Perform linear static analysis:
   - define line-type system and apply load case LC1,
2. Perform linear bifurcation analysis (LBA):
   - define line system for buckling evaluation,
   - use load case LC101 and calculate the first 10 buckling mode shapes,
3. Define geometric imperfection based on buckling mode:
   - apply imperfection using mode shape from LC101,
   - scale the amplitude of the out-of-plane buckling mode to 59.60 mm,
   - store as imperfection case LC202,
   - set numerical tolerance for convergence: dlz = 1E-4,
4. Execute full nonlinear analysis with both imperfections:
   - use TH3 solver for iterative computation (max 200 iterations),
   - enable nonlinear behavior for material and stiffness,
   - apply in-plane imperfection scaled to 52.50 mm using LC103,
   - define total load case LC202,
   - combine with load case LC1,
5. Close program.

4.4. Comparison of the forms of arch stability loss

Figure 13 presents a spatial model of the designed object, which was developed in program [16]. This model accurately reflects the actual structural system by incorporating the material properties and stiffness of the elements, which enables precise analysis of the structure's behavior under the influence of loads.

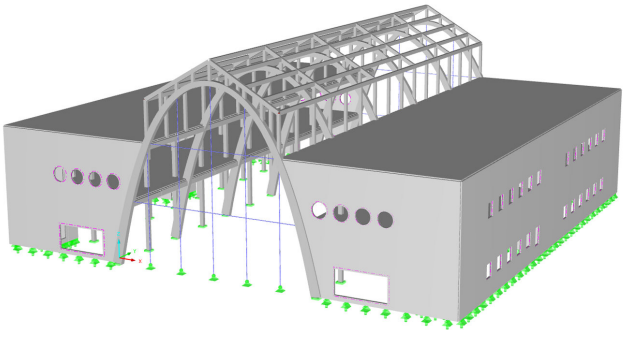

Fig. 13. Computational spatial model of the structure

The model was created to dimension the remaining structural elements and to verify the validity of the assumptions adopted for the model in program [11]. The spatial model, in particular, accounted for the influence of the structure's stiffness distribution and the interactions between its elements. This made it possible to verify the adopted boundary conditions and to assess their compliance with the structure's actual operating conditions.

The following load cases were considered in the model:

- self-weight,
- dead load,
- suspended load,
- live load of the ceiling – load on the entire surface,
- live load of the ceiling – band load scheme (inner span),
- live load of the ceiling – band load scheme (extreme span),
- live load – mixed band scheme (inner span),
- live load – mixed band scheme (extreme span),
- snow load – load of the side aisles, including snowdrifts,
- snow load – load on the entire surface of the side aisles,
- snow load – uniform load of the main nave,
- snow load – uneven load of the main nave, one slope more heavily loaded,
- snow load – uneven load of the main nave, second slope more heavily loaded,
- wind load in the positive direction of the X-axis,
- wind load in the negative direction of the X-axis,
- wind load in the positive direction of the Y-axis,
- wind load in the negative direction of the Y-axis.

The results of the computational analysis conducted in program [16] were the internal force values obtained by considering the selected load combinations. These results were used to dimension the main load-bearing structure in program [11]. A high consistency in the predicted modes of arch stability loss was observed between two independent numerical programs [11, 16], supporting the validity of the adopted boundary conditions and the modeling of support flexibility as implanted in software [11]. This agreement is illustrated in Figs. 14–18, which present a side-by-side comparison of the critical buckling modes obtained from both computational approaches. The qualitative similarity of the critical modes further validates the robustness of the structural idealization and justifies the assumptions adopted in nonlinear analysis.

- Mode No. 1 – out-of-plane buckling

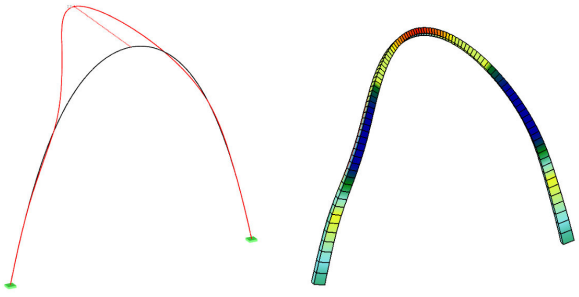

(a) (b)

Fig. 14. First buckling mode of the arch: (a) spatial model, (b) planar mode

- Mode No. 2 – out-of-plane buckling

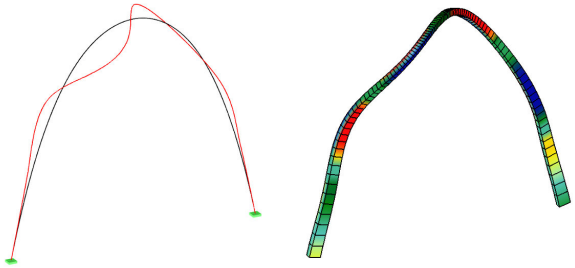

(a) (b)

Fig. 15. Second buckling mode of the arch: (a) spatial model, (b) planar mode

- Mode No. 3 – in-plane buckling

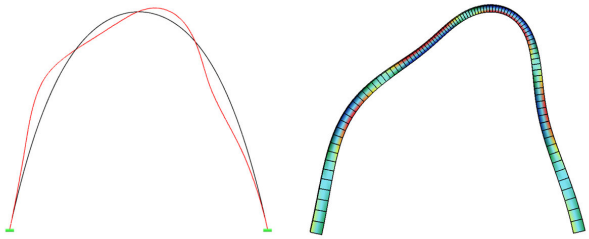

(a) (b)

Fig. 16. Third buckling mode of the arch: (a) spatial model, (b) planar mode

- Mode No. 4 – out-of-plane buckling

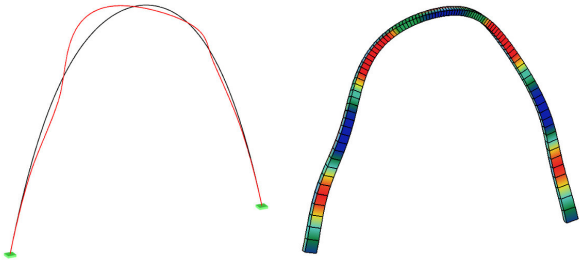

(a) (b)

Fig. 17. Fourth buckling mode of the arch: (a) spatial model, (b) planar mode

- Mode No. 5 – out-of-plane buckling

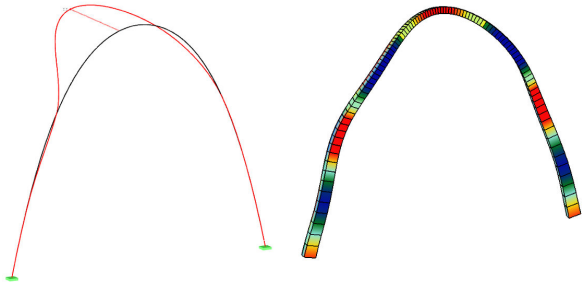

(a) (b)

Fig. 18. Fifth buckling mode of the arch: (a) spatial model, (b) planar mode

The calculation results in the form of extreme internal forces and nodal displacements are derived from a full nonlinear geometric and material analysis taking into account the influence of external loads, self-weight, second-order effects, geometric imperfections in and off the plane of the arch, the influence of long-term creep and shrinkage of concrete, as shown in Figs. 19–20.

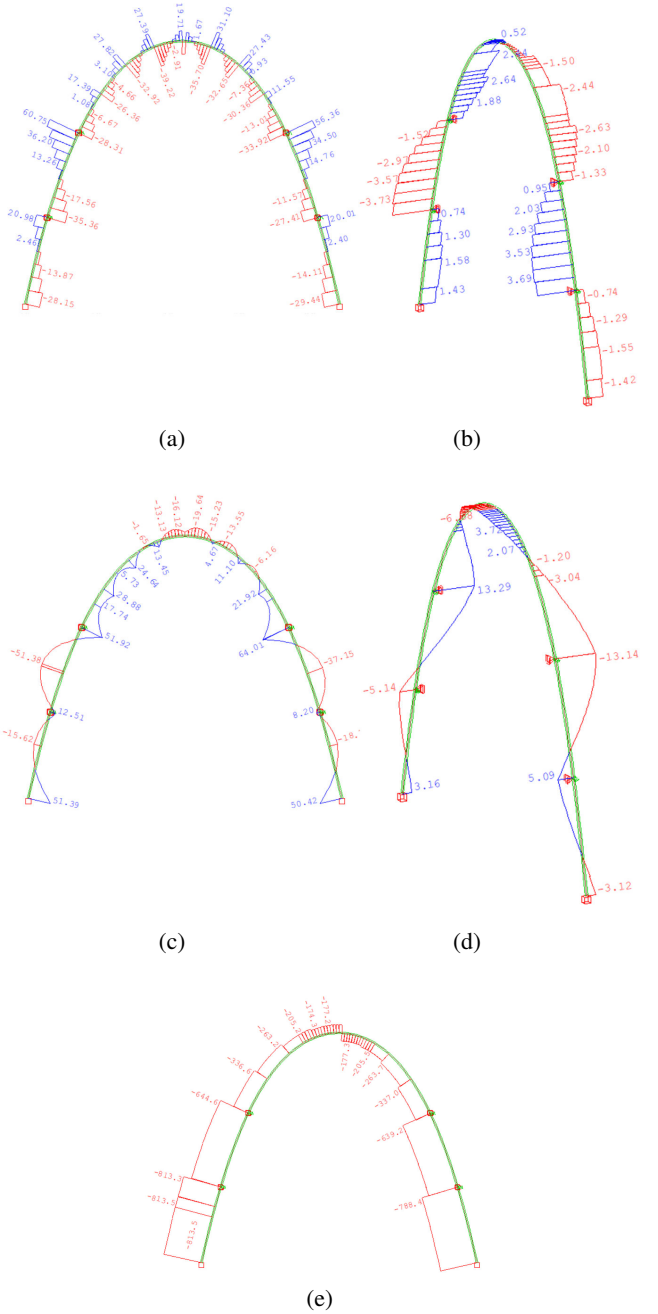

(a) (b) (c) (d) (e)

Fig. 19. Distribution of internal forces in the arch structure: (a) shear forces V_z [kN], (b) shear forces C_y [kN], (c) bending moments M_y [kNm], (d) bending moments M_z [kNm], (e) axial forces N_x [kN]

Figure 21a shows the location of characteristic cross-sections along the arch where stress concentrations were observed. The corresponding axial strains in these sections are illustrated in Fig. 21b.

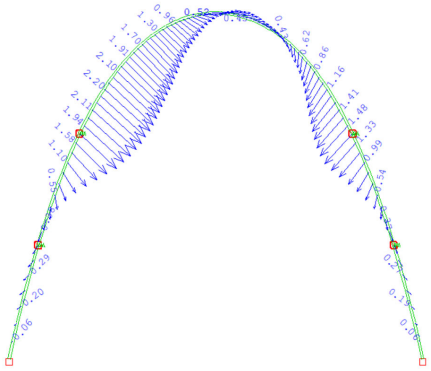

Fig. 20. Nodal displacements [mm]

(a) (b)

Fig. 21. Axial deformation analysis in the arch structure: (a) location of characteristic cross-sections, (b) axial deformations in corresponding cross-sections [‰]

The associated stress values were determined based on the adopted nonlinear material model in the σ-ε domain. The maximum axial strain in the cross-section under combined loading is $\varepsilon = 0.263‰$, which corresponds to a compressive stress of $\sigma_c = 2.81$ MPa. Maximum tensile stress reaches $\sigma_t = 1.10$ MPa $\leq f_{ct,\text{eff}} = 1.45$ MPa, remaining below the effective tensile strength of concrete C30/37. Consequently, the section remains uncracked.

5. CONCLUSIONS

The method applied, which combines the funicular design approach with nonlinear numerical analysis, enabled the determination of an arch shape optimally aligned with internal force distributions. As a result, significantly lower values of bending moments and shear forces were obtained, which considerably simplified the dimensioning process. Consequently, load-bearing reinforcement was found to be unnecessary, and only the minimal structural reinforcement required by Eurocode 2 was provided. The analysis revealed that the main load-bearing structure primarily experiences compressive forces, confirming the assumptions of the method adopted. This allows for more efficient use of construction materials, making the designed object both cost-effective and durable, which is particularly relevant for sustainable urban infrastructure.

The obtained displacements of the structure are small, amounting to 2 mm, which indicates the high stiffness and stability of the system. This is crucial for the long-term operation of the structures in urban areas, where durability and minimal maintenance requirements are key factors in public infrastructure and historic preservation. By minimizing displacements, the risk of secondary damage, such as cracks or scratches, is significantly reduced, ensuring long-term resilience in urban environments.

A comparison of the results obtained using graphic statics and the finite element method confirms the effectiveness of the adopted design approach. The agreement between the numerical analysis results and the theoretical assumptions of the funicular method confirms the accuracy of both the calculation model and the design assumptions.

The methodology presented herein illustrates how the integration of traditional structural principles with advanced numerical techniques supports the digital transformation of the architectural and structural design process. The proposed approach facilitates the development of reinforced concrete structures optimized in terms of load-bearing performance, stiffness and material efficiency. In doing so, it addresses key priorities in sustainable construction, including the reduction of embodied carbon and the implementation of low-carbon design strategies.

In a broader context, this method contributes to the creation of resource-efficient, climate-resilient structures that meet the evolving needs of urban environments. It also demonstrates the potential of digitally supported structural shaping to advance sustainable development goals and to support the transformation of cities into more environmentally responsible, durable and adaptive systems.

ACKNOWLEDGEMENTS

The author gratefully acknowledges the support received under the project "U-team! An Alliance of European Universities for Building a Joint Educational Offer and Conducting Research", implemented by Wrocław University of Science and Technology within the NAWA program "Support for European Universities", co-funded by the European Funds for Social Development (FERS). The author also expresses his gratitude to the Wrocław University of Science and Technology working group for participation in the research visit to Technische Universität Darmstadt. The scientific discussions held with Professor Dr.ir. Eddie Koenders and Dr. Chem. Ing. Neven Ukrainczyk from the Institute of Construction and Building Materials at TU Darmstadt provided valuable inspiration and perspectives, which were considered during the correction of this article and significantly contributed to its final quality.

FUNDING INFORMATION

This article has been supported under the European Funds for Social Development (FERS) program and the Support for Alliances of European Universities NAWA program numbered BPI/WUE/2024/1/00031/DEC/1.

REFERENCES

[1] F. Aram, "Sustainable Design in Building and Urban Environment," *Designs*, vol. 7, no. 4, p. 99, 2023, doi: 10.3390/designs7040099.

[2] J. Szafran, A. Zingoni, M.P. Repetto, and M. Kamiński, "Lightweight structures in civil engineering – contemporary problems," *Bull. Pol. Acad. Sci. Tech. Sci.*, vol. 71, no. 1, p. e144589, 2023, doi: 10.24425/bpasts.2023.144589.

[3] A.R. Kulkarni and V. Bhusare, "Structural optimization of reinforced concrete structures," *Int. J. Eng. Res. Technol.*, vol. 5, no. 7, pp. 123–127, 2016, doi: 10.17577/IJERTV5IS070156.

[4] E. Allen, W. Zalewski, and Boston Structures Group, *Form and Forces: Designing Efficient, Expressive Structures*. Oxford: John Wiley & Sons, 2010.

[5] S. Stevin, *Hypomnemata Mathematica*, vol. 1. Patius, 1608.

[6] P. Varignon, *Nouvelle mécanique ou statique: dont le projet fut donné en MDCLXXXVII*, vol. 2. Paris: Claude Jombert, 1725.

[7] P. Block, M. DeJong, and J. Ochsendorf, "As hangs the flexible line: equilibrium of masonry arches," *Nexus Netw. J.*, vol. 8, no. 2, pp. 13–24, 2006.

[8] H. Rozendaal and A. Borgart, "Calculating arches through graphic statics: developing a new method," in *Proc. IASS Symp.*, 2015, pp. 1–10.

[9] G. Tempesta and S. Galassi, "Safety evaluation of masonry arches. A numerical procedure based on the thrust line closest to

the geometrical axis," *Int. J. Mech. Sci.*, vol. 155, pp. 206–221, 2019, doi: 10.1016/j.ijmecsci.2019.02.036.

[10] S. Galassi and G. Tempesta, "The MatLab code of the method based on the Full Range Factor for assessing the safety of masonry arches," *MethodsX*, vol. 6, pp. 1521–1542, 2019, doi: 10.1016/j.mex.2019.05.033.

[11] SOFiSTiK (Teddy), 2023. [Online]. Available: https://www.sofistik.com/ (Accessed: 18 Jan. 2025).

[12] European Committee for Standardization, Eurocode 2: Design of Concrete Structures – Part 1-1: General Rules and Rules for Buildings, EN 1992-1-1:2004.

[13] European Committee for Standardization, Eurocode 5: Design of Timber Structures – Part 1-1: General – Common Rules and Rules for Buildings, EN 1995-1-1:2004+A1:2008.

[14] European Committee for Standardization, *Eurocode 3: Design of Steel Structures – Part 2: Steel Bridges*, EN 1993-2:2006.

[15] European Committee for Standardization, Eurocode 2 – Design of Concrete Structures. Part 1-1: General Rules and Rules for Buildings, Bridges, and Civil Engineering Structures, EN 1992-1-1:2023.

[16] Dlubal RFEM 5.34. [Online]. Available: https://www.dlubal.com/ (Accessed: 18 Jan. 2025).

[17] O. Iuorio, "BIM, free form shells and digital fabrication," in *The Changing Architect*. Maggioli Editore, Mar. 2018.

[18] T. Srisuwan, "Structural Morphology: An Effective Solution for Generating Efficient Structural Forms," *BUILT*, vol. 18, pp. 7–22, 2023.

[19] S. Huerta, "Structural design in the work of Gaudí," *Archit. Sci. Rev.*, vol. 49, no. 4, pp. 324–339, Dec. 2006, doi: 10.3763/asre.2006.4943.

[20] J. Ilkosz, R. Wójtowicz, and J. Urbanik, "New form, new material and color scheme, the exposed concrete phenomenon – the Centennial Hall in Wrocław," *Arts*, vol. 11, no. 1, p. 17, 2022, doi: 10.3390/arts11010017.

[21] P. Berkowski and G. Dmochowski, "Examples of concrete structural elements in early 20th century buildings in Wrocław (Poland) – case studies," in *Concrete Solutions 2014: Proceedings of the 5th International Conference on Concrete Repair*, 2014, doi: 10.1201/b17394-108.

[22] M. Licordari, "The Centennial Hall of Wroclaw: history of a modern architecture in reinforced concrete classified World Heritage Site," *J. Archit. Conserv.*, vol. 27, no. 1–2, pp. 17–52, 2021, doi: 10.1080/13556207.2020.1854508.

[23] S. Wimalasena, T.G. Weerakoon, and J. Wimalasena, "Integrated approaches to sustainable urban development: the synergy between landscape architecture and civil engineering," *Sci. Future Lith.*, vol. 17, pp. 1–17, 2025, doi: 10.3846/mla.2025.22836.

[24] N.M.K. Narasimha, E.M.M. Beevi, P.P. Nelda, and H.K. Thejas, "Cost optimization and estimation of embodied carbon in reinforced concrete frame structure," *Sustain. Agri Food Environ. Res.*, vol. 12, 2024, doi: 10.7770/safer-V12N-art780.

[25] X. Zhang and X. Zhang, "Low-carbon design optimization of reinforced concrete building structures using genetic algorithm," *J. Asian Archit. Build. Eng.*, vol. 23, no. 6, pp. 1888–1902, 2024, doi: 10.1080/13467581.2023.2278466.

[26] E. Allen and W. Zalewski, *Shaping Structures: Statics*. New York: John Wiley & Sons, 1998.

[27] J. Červenka, J. Rymeš, L. Jendele, and R. Pukl, "Is Nonlinear Analysis Becoming a Standard Tool for Design and Assessment of Reinforced Concrete Structures?" in *Proc. IABSE Congr., New Delhi 2023: Engineering for Sustainable Development*, pp. 1585–1592, 2023, doi: 10.2749/newdelhi.2023.1585.

[28] European Committee for Standardization, Eurocode 1: Actions on Structures – Part 1-1: General Actions – Densities, Self-weight, Imposed Loads for Buildings, EN 1991-1-1:2002.

[29] European Committee for Standardization, Eurocode 1: Actions on Structures – Part 1-3: General Actions – Snow Loads, EN 1991-1-3:2003.

[30] European Committee for Standardization, Eurocode 1: Actions on Structures – Part 1-4: General Actions – Wind Actions, EN 1991-1-4:2005+A1:2010.

[31] Wolfram Mathematica. [Online]. Available: https://www.wolfram.com/ (Accessed: 18 Jan. 2025).